Advanced Materials Research *Online: 2014-08-11*
ISSN: 1662-8985, Vol. 996, pp 833-840
doi:10.4028/www.scientific.net/AMR.996.833

On-chip MEMS-based internal stress actuated structures for the mechanical testing of freestanding thin film materials

Renaud Vayrette[1,2,a*], Michael Coulombier[2,b], Thomas Pardoen[1,3,c] and Jean-Pierre Raskin[2,3,d]

[1]Institute of Mechanics, Materials and Civil Engineering, Université catholique de Louvain, 1348 Louvain-la-Neuve, Belgium

[2]Institute of Information and Communication Technologies, Electronics and Applied Mathematics, Université catholique de Louvain, 1348 Louvain-la-Neuve, Belgium

[3]Research Center in Micro and Nanoscopic Materials and Electronic Devices, Université catholique de Louvain, 1348 Louvain-la-Neuve, Belgium

[a]renaud.vayrette@uclouvain.be, [b]michael.coulombier@uclouvain.be
[c]thomas.pardoen@uclouvain.be, [d]jean-pierre.raskin@uclouvain.be

Keywords: thin film, internal stress, on-chip mechanical testing

Abstract. An on-chip suite of MEMS-based mechanical testing structures has been developed to extract the mechanical properties of freestanding thin films under tensile loading. The working principle relies on the use of high tensile internal stress within an actuator beam to deform a specimen beam made of another material owing to the etching of an underlying sacrificial layer. In order to control the deformation rate imposed during the etching process, the rectangular shape of actuator beam design has been recently upgraded to a tapered shape. The deformation rate is estimated from the modelling of the two extreme cases defining the upper and lower limit. The proof of concept is demonstrated experimentally from the investigation of the mechanical response of 100 nm-thick freestanding copper thin films deposited by e-beam evaporation.

Introduction

The expansion of practical applications using nano-objects such as thin films, nano-wires, dots and nano-particles is frequently impeded by mechanical reliability issues. In order to design and fabricate reliable devices, the characterization and understanding of the mechanical response of nano-objects are of prime interest.

On-chip MEMS-based mechanical testing methods are particularly powerful to probe the mechanical properties of freestanding nano-objects. They take benefit of nano- and micro-fabrication techniques which are (1) the capacity to reproduce of a large number of elementary planar patterns from the deposition and the etching of a thin film material; (2) the capacity to fabricate complex three dimensional structures from the optimized stacking of elementary patterns of different materials; (3) the fact that it can avoid, partly or entirely, the manipulation of the test objects and the use of macroscopic actuating and sensing devices.

Numerous designs of structures with varying complexity have been developed over the years to produce dynamic and quasi static mechanical tests. For quasi static mechanical test systems, two main groups emerge: the simple elementary structures and the complex stages with an advanced design.

The simple elementary structures are usually dedicated to the extraction of one specific mechanical property in the elastic regime such as the mismatch strain [1,2], the residual stress [3,4] and the Young's modulus [5,6]. The fabrication process is relatively straightforward because it involves a limited number of processing steps. The principle is to induce a measurable displacement by changing the mechanical equilibrium in a freestanding structure. The experimental displacement is measured with a Scanning Electron Microscope (SEM), with a nano-instrumented sensing system

or by interferometry. The output parameter is computed with analytical model based on beam theory or a finite elements simulation describing the mechanical behavior of the structure. The actuation can be provided by an external device such as with the tip of a nano-indentor [5] or with an Atomic Force Microscope (AFM), or with an electrical signal inducing an electrostatic effect [4,6]. Another concept of actuation consists in converting the internal stress relaxation of a structure in a measurable displacement owing to an optimized design and to the etching of an underlying sacrificial layer [1,2,3]. The freestanding structure relaxes elastically until reaching mechanical equilibrium. No external actuation is required. In order to improve the robustness of the extraction method, structures with different in-plane dimensions are used to probe several mechanical equilibrium states.

By contrast, the complex stages are devoted to the characterization of the entire mechanical response of freestanding thin films under uniaxial tensile loading as well as during unloading. The mechanical testing is performed in a Transmission Electron Microscope (TEM) or in a SEM for the in-situ investigation of the deformation mechanisms. The processing involves a large number of steps because the specimen, the actuation and the sensing structures are co-fabricated during the same process flow. The loading and unloading is produced by the use of an electrical signal inducing piezo-resistive [7], electrostatic [8] or electrothermal actuation [9]. The stiffness of the actuation and sensing structures has to be calibrated by finite elements simulations so as to extract accurately the stress and the strain in the specimen beam. The fabrication, the use and the interpretation of experimental data (force and displacement) are more complicated than for simple elementary structures.

In order to circumvent the use of an external actuator and to minimize the design complexity as well as the number of processing steps, the concept of internal stress actuated structures has been extended to uniaxial tensile tests [10]. The method is based on two key ideas: (1) the use of the high tensile internal stress present in a silicon nitride beam to deform another specimen beam attached to it owing to the etching of a sacrificial layer, (2) the use of a large number of simple elementary testing structures with different in-plane dimensions so as to extract the complete specimen stress-strain curve instead of building a simple complex stage. This concept has been successfully applied on brittle [11,12] and ductile films [10,11,13,14] with a thickness between 50 and 1000 nm for the characterization of the tensile mechanical response as well as the creep/relaxation behavior [14].

Recently, the structures design has been upgraded. The classic rectangular actuator design has been substituted by a tapered shape allowing the control and the estimation of the specimen strain rate. This paper aims to introduce and validate the working principle of the upgraded structures design from the investigation of the mechanical response of 100 nm-thick freestanding copper films. It allows also covering the key ideas of the method which is still rather in its infancy and presenting some new results on freestanding copper films.

The outline of the paper is as follows. The basic principles of the on-chip internal stress actuated testing structures and the modelling strategies developed for the estimation of the strain rate are presented first. Then, the samples processing and design are described. Finally, the experimental stress-strain curves of a 100 nm-thick Cu films extracted with classic and upgraded structures are exposed to illustrate the proof of concept and estimate the specimen strain rate.

On-chip internal stress actuated mechanical testing concept

Principle. One testing structure is composed of two beams deposited on a sacrificial layer: one actuator beam made of silicon nitride involving a large tensile internal stress and one specimen beam (Fig. 1). The connection between both beams is ensured by an overlapping region. At the specimen beam ends, dogbone shapes are located to concentrate the loading where the width is uniform. The mechanical loading of the specimen beam occurs during the etching of the underlying sacrificial layer named the release step.

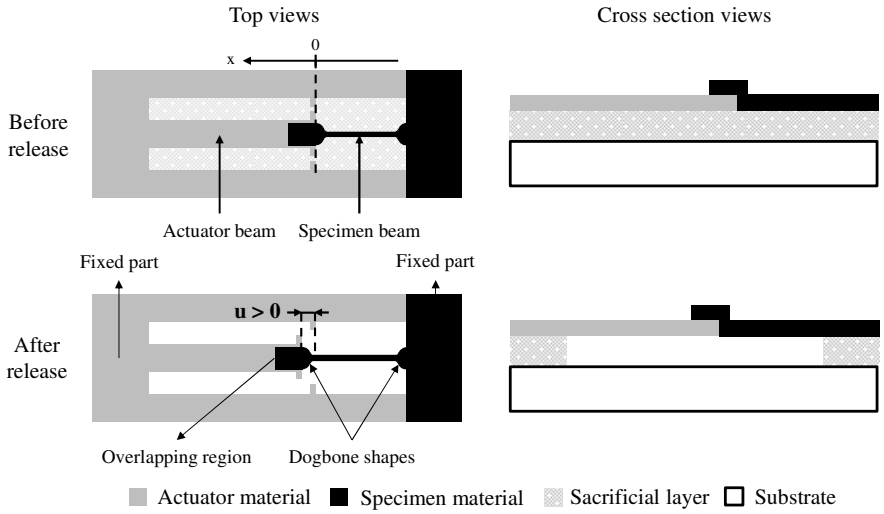

Fig. 1. Top and cross-sectional views of an on-chip uniaxial tensile testing structure before and after the release step.

Before the release step, the actuator and specimen materials are pre-deformed due to the stress developing during processing, leading to mismatch strains ε_a^{mis} and ε^{mis}, respectively. By definition, the mismatch strain is equal to minus the elastic strain stored in a material and is negative for a tensile internal stress. Let us assume that the specimen material involves a tensile initial internal stress. From Hooke's law, the initial forces in the actuator and specimen beams, respectively F_{a0} and F_0, are expressed as

$$F_{a0} = -S_{a0} E_a \varepsilon_a^{mis}, \tag{1}$$

$$F_0 = S_0 E \varepsilon^{mis}, \tag{2}$$

where S_{a0} is the cross sectional area of the actuator beam, S_0 is the cross sectional area of the specimen beam, E_a is the Young's modulus of the actuator material, and E is the Young's modulus of the specimen material. In order to enforce the deformation of the specimen beam during the release step, the dimensions of the actuator and specimen beams (length, width and thickness) are set to satisfy the relation $F_{a0} > |F_0|$ (Fig. 2).

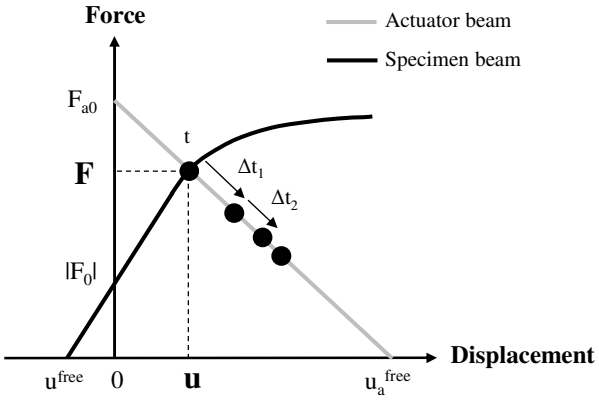

Fig. 2. Force-Displacement diagram for the actuator and specimen beams.

During the release step, the actuator beam force relaxes elastically acting as a spring while the specimen beam force increases until the establishment of mechanical equilibrium. After the release step, the forces in both beams are equal to F as $F_{a0} \geq F \geq 0$. The referring displacement u is $0 \leq u \leq u_a^{free}$, with 0 corresponding to the initial state ($F = F_{a0}$), and u_a^{free} being the potential maximum displacement which could be imposed by a fully relaxed actuator beam ($F = 0$). The specimen stress

and strain are extracted from the measurement of the displacement u of cursors with a SEM and the use of a data reduction scheme based on beam theory which has been detailed in [11]. The expressions of the stress σ and strain ε in the specimen are given by

$$\sigma = E_a \varepsilon_a \frac{S_a}{S} = E_a \left(-\varepsilon_a^{mis} - \frac{u}{L_{a0}} \right) \frac{S_a}{S}, \tag{3}$$

$$\varepsilon = \ln\left(1 + \frac{u}{L_0} \right) - \varepsilon^{mis} \approx \frac{u}{L_0} - \varepsilon^{mis}, \tag{4}$$

where S_a and S are, respectively, the cross sectional area of the actuator and specimen beam after the release step, and L_{a0} and L_0 are, respectively, the actuator and specimen beam length before the release step. The logarithm form of Eq. (4) is appropriate to the general case of large deformations and the linear form refers to the small strain approximation. The extraction of specimen stress σ and strain ε with, respectively, Eq. 3 and Eq. 4 requires knowing with accuracy the geometrical features of the specimen and actuator beams (width, length and thickness) as well as the mechanical quantities ε_a^{mis}, E_a and ε^{mis}. All these input parameters are extracted after the released step for each sample. The actuator and specimen widths are measured with a SEM. The actuator and specimen thicknesses measurements are performed on squares of ~1 mm x 1 mm, respectively, by ellipsometry and/or mechanical profilometry. The mismatch strains ε_a^{mis} and ε^{mis} are extracted from the use of simple elementary on-chip test structures using the actuation concept based on the internal stress relaxation: the self-actuated structures [2], the rotating sensors [1] and/or the free cantilevers [2]. The actuator Young's modulus E_a is computed by combining the equi-biaxial internal stress obtained by curvature measurements $\sigma_{biaxial}$ and the mismatch strain ε_a^{mis} [2].

From the experimental cursors displacement belonging to one test structure, one point of the stress-strain curve is extracted. By varying the in-plane dimensions of the actuator and the specimen beams, different strain and stress levels are probed allowing the extraction of the entire discrete specimen strain-stress curve from small strain up to failure.

For some specimen materials such as ductile metals and polymers, creep/relaxation phenomena can be active directly after the release step depending on the stress level, temperature, microstructure, thickness and external surface state. In this case, the specimen beam stress decreases while the specimen beam strain increases following the linear force – displacement characteristic imposed by the actuator beam (Fig. 2). As a consequence, the stress and strain response does not correspond to the mechanical state directly after the release step but to the mechanical state at the time of the displacement measurement. Similarly, the creep/relaxation behavior can be investigated by monitoring the evolution of the displacement u with time [14].

Thanks to the use of micro- and nano-fabrication techniques, thousands of tests using a single processed wafer can be performed making statistical data analysis possible.

Tapered actuator design for the control of the specimen strain rate. The classic design of structures involves actuator beams with rectangular shape (Fig. 1). For a constant sacrificial layer etching rate v, a perfect rectangular actuator beam of width w_a becomes instantaneously freestanding at the same time t_1 equal to $v/(2w_a)$. In reality, the local chemical composition and density of the sacrificial layer change leading to variability of local etching rates. During the release step, some regions of the actuator beam become freestanding while others are always attached to the substrate. The release of actuator beam and the specimen mechanical loading are then sequential, uncontrolled and probably very fast. In order to solve these issues, structures with a tapered shape actuator have been produced in the last generation of our on-chip test method. Fig. 3 is a schematic drawing of a structure with a tapered actuator of maximum width $w_{a\,max}$, minimum width $w_{a\,min}$ and length L_{a0}.

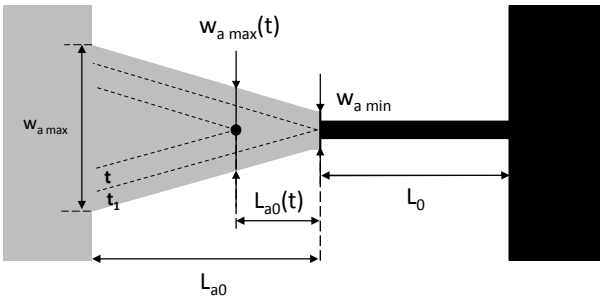

Fig. 3. Schematic drawing of a structure with a tapered actuator design for controlling the specimen strain rate.

The mechanical loading starts at time t_1 and stops at time t_f which are the durations required to etch a length of, respectively, $w_{a\,min}/2$ and $w_{a\,max}/2$. For $t > t_1$, the in-plane dimensions of a free tapered actuator, $w_{a\,max}(t)$ and $L_{a0}(t)$, increase linearly with time:

$$w_{a\,max}(t) = 2vt, \tag{6}$$

$$L_{a0}(t) = L_{a0}\left(1 - \frac{w_{a\,max} - 2vt}{w_{a\,max} - w_{a\,min}}\right). \tag{7}$$

Therefore this simple design modification allows progressively relaxing the internal stress of actuator beam during the release step. As the actuator width evolves linearly from $w_{a\,max}$ to $w_{a\,min}$, the specimen stress and strain can be computed using Eq. 3 and Eq. 4, respectively. The actuator cross-sectional area S_a injected in Eq. 3 is the product of the actuator thickness h_a and the average free actuator beam width $w_a(t) = (w_{a\,max}(t) - w_{a\,min})/2$.

In order to estimate the strain rate, two modelling approaches corresponding to two extreme cases have been developed in the small strains formulation. The first approach consists in expressing the specimen strain rate from the maximum displacement of an actuator beam fully relaxed ($\varepsilon_a(t) = 0$) of length $L_{a0}(t)$ and mismatch strain ε_a^{mis}. Eq. 8 constitutes the expression of the upper limit of the strain rate:

$$\dot{\varepsilon} = \frac{1}{L_0}\frac{du}{dt} = -\varepsilon_a^{mis}\frac{L_{a0}}{L_0}\left(\frac{2v}{w_{a\,max} - w_{a\,min}}\right). \tag{8}$$

In this case, the strain rate is time independent. It increases linearly with ε_a^{mis}, v, L_{a0}/L_0 and is inversely proportional to $w_{a\,max} - w_{a\,min}$.

The second approach consists in expressing the specimen strain rate from a pure elastic formalism of mechanical equilibrium at each time t (Eq. 9).

$$\dot{\varepsilon} = \frac{1}{L_0}\frac{du}{dt} = \frac{1}{L_0}\frac{BdA - AdB}{B^2} \quad \text{with } u(t) = \frac{A}{B} = \frac{ES\varepsilon^{mis} - \varepsilon_a^{mis}E_a h_a\left[vt + \frac{w_{a\,min}}{2}\right]}{\frac{ES}{L_0} + E_a h_a \frac{w_{a\,max} - w_{a\,min}}{L_{a0}}\frac{vt + w_{a\,min}/2}{2vt - w_{a\,min}}}. \tag{9}$$

In this case, the strain rate evolves with time as well as the geometrical and material features of the actuator and specimen beams. The evaluation of the lower limit of the strain rate with Eq. 9 requires to know E. As a consequence, the specimen strain rate is only estimated after the extraction of the specimen stress-strain curve.

Samples processing and design

The processing involves the successive deposition and patterning of three thin film materials on the top of a 3-inch silicon wafer: the silicon oxide sacrificial layer, the silicon nitride actuator and the copper specimen materials. First, a 1 µm-thick silicon oxide is deposited by Plasma Enhanced Chemical Vapor Deposition at 300 °C and 675 mTorr with gas flow of $SiH_4/N_2O/N_2$ in the proportion of 100/700/350 sccm. Then, a 60 nm-thick silicon nitride film is deposited by Low Pressure Chemical Vapor Deposition at 790 °C and 250 mTorr with gas flow of SiH_2Cl_2/NH_3 in the proportion of 75/49 sccm. This layer is patterned by photolithography and a SF_6 plasma etching. Finally, a lift-off technique is used for the successive depositions by e-beam evaporation of a non-conformal layer of titanium clusters and a 100 nm-thick copper film. The non-conformal layer of titanium clusters is deposited first to ensure the adhesion of the overlapping region between the copper and the silicon nitride beams. The depositions are performed at room temperature with a pressure ~0.1 mTorr. The deposition rate is 1 $A.s^{-1}$.

Two different designs of structures have been produced and investigated for the extraction of the stress-strain curve of the 100 nm-thick freestanding copper film. The first design corresponds to the classic structures with a rectangular actuator named R series. The second design corresponds to the upgraded structures with a tapered actuator named T series. All the structures have been designed on the same masks set so as to be processed on the same wafer and to probe the mechanical properties of the same specimen thin film. The R series involve 30 structures with a constant total structure length, i.e., the actuator beam length plus the specimen beam length, of 2,000 and 1,000 µm. Within one set of structures, the ratio of lengths between the specimen beam and actuator beam L_{a0}/L_0 are varied from 0.3 to 50, the specimen tensile loading increasing with L_{a0}/L_0. The actuator beam and specimen widths are equal to 10 µm and 2 µm, respectively. A set of structures is named 'Ra b c', a being the actuator beam width, b being the specimen beam width and c being the total length. The T series involve 20 structures with a constant specimen beam length of 400 µm and width of 2 µm. Within one set of structures, the ratio L_{a0}/L_0 is varied from 0.25 to 3.1. The maximum actuator width is 20 µm and the minimum actuator width is 10 µm. A set of structures is named 'Td e f', d being the actuator beam width, e being the specimen beam width and f being the specimen beam length. Three sets of structures have been investigated: T15 2 400, R10 2 2000 and R10 2 1000.

The structures are released by wet etching in a 73% pure hydrofluoric acid. The etching time is equal to 1 min 40 s for the R series and 2 min for the T series. The etching time has been set from the preliminary estimation of the sacrificial layer etching rate which is v = 0.105 µm.s^{-1}. In order to keep the released structures freestanding and avoid their stiction onto the underlying substrate, they are rinsed first with deionized water and then with iso-propanol during 15 min before being dried with a Critical Point Dryer. The first measurement with a SEM is done ~1 h after the release step.

Results

The mismatch strain of 60 nm-thick silicon nitride films ε_a^{mis} extracted through the use of six to ten self-actuated structures (depending on the sample) is -0.318 +/- 0.001%. The equi-biaxial stress $\sigma_{biaxial}$ determined from the curvature measurements of 3 wafers fabricated during the same process flow is equal to 985 +/- 110 MPa. By combining $\sigma_{biaxial}$ and ε_a^{mis}, the computed Young's modulus of silicon nitride film is equal to 240 +/- 31 GPa. The mismatch strain of the 100 nm-thick copper thin film ε^{mis} extracted from the displacement of 4 single clamped cantilevers is -0.1% +/- 0.01%.

Fig. 5 (a) shows the stress-strain curves of 100 nm-thick freestanding copper films extracted from the investigation of the R and T series. The three stress-strain curves are superposed. No strain rate sensitivity effect is observed between the R and T series. It indicates that the possible changes of resistance due to the different strain rate have disappeared after a time of 1 h which corresponds to the time between the etching and the first measurement. The error bars for the stress level and the strain are not shown for clarity. They are determined by analyzing the error propagation in Eq. 3 and Eq. 4 using $\Delta w = \Delta u = 0.05$ µm, $\Delta h_a = \Delta h = 5$ nm and $\Delta L = 1$ µm. For the R and T series, the error

on the strain is equal to 0.025 %. The error on the stress levels is roughly constant. It is estimated to +/- 35 MPa and +/- 60 MPa for, respectively, the R and T series. The experimental stress-strain curves exhibit a Young's modulus of ~110 GPa and a yield strength equal to ~200 MPa. The set of structures R10 2 1000 presents the maximal ultimate fracture strain and stress which are, respectively, ~1.4 % and ~350 MPa. For the T series structures, the ratio L_{a0}/L_0 is not large enough to induce the fracture of the specimens.

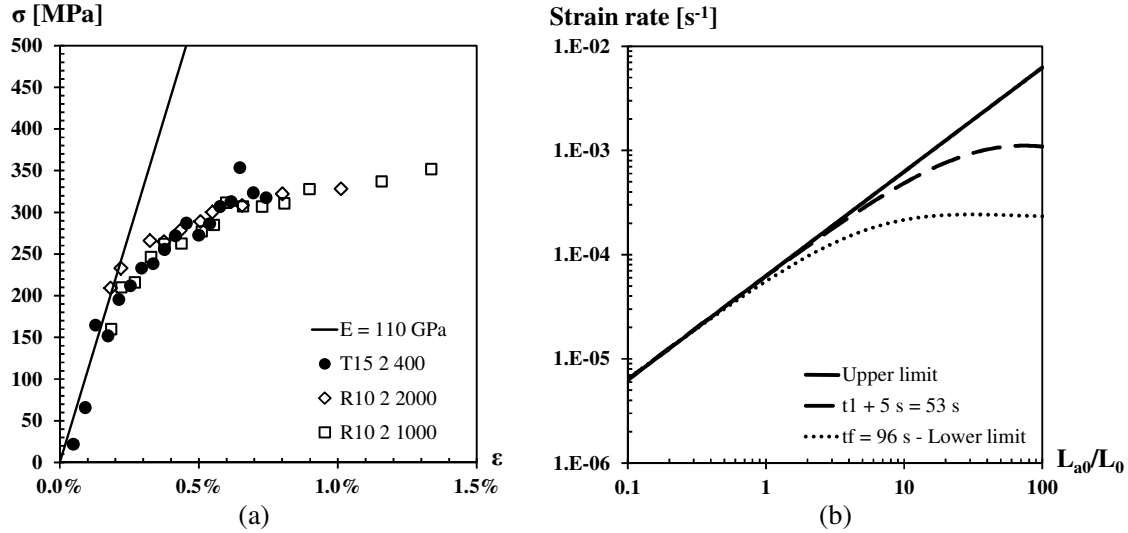

Fig. 5. (a) Stress-strain curves of 100 nm-thick freestanding copper films of width 2 µm. The empty points correspond to the data extracted with the structures of the R series. The filled points correspond to the data extracted with the structures of the T series.
(b) Plot of the strain rate associated to the set of structures T15 2 400 as a function of the ratio of L_{a0}/L_0. The straight line is computed with Eq. 8. The dashed and dotted lines are calculated with Eq. 9 for, respectively, $t = t_1 + 5$ s and $t = t_f$.

Fig. 5 (b) shows the specimen strain rates as a function of L_{a0}/L_0. The specimen mechanical loading starts at $t_1 = 48$ s and ends at $t_f = 96$ s. As expected, the strain rate increases with L_{a0}/L_0. For $L_{a0}/L_0 < 1$, the two modelling approaches lead to very close results. The specimen strain rate increases linearly with the increase of L_{a0}/L_0 and can be considered as time independent. It is about $1.5\text{x}10^{-5}$ s^{-1} for $L_{a0}/L_0 = 0.25$ and reaches $6\text{x}10^{-5}$ s^{-1} for $L_{a0}/L_0 = 1$. For $L_{a0}/L_0 > 1$, the two modelling approaches diverge with time. In the beginning of the mechanical loading, the strain rate is maximum and is equal to the upper limit. The strain rate computed with Eq. 9 decreases as a function of time and reaches a minimum value at the end of the mechanical loading $t = t_f$ defining the lower limit. For $L_{a0}/L_0 = 3.1$, it is comprised between $1.3\text{x}10^{-4}$ s^{-1} and $1.9\text{x}10^{-4}$ s^{-1}. The estimation of the strain rates reveals one decade increase between the values associated to the first and the last structures of the R series investigated in this work. Besides, the difference between the upper and lower limits of the strain rate rises as L_{a0}/L_0 increases. It becomes particularly high for structures with large L_{a0}/L_0 ratio. In our specific configuration, one decade difference (from $2.4\text{x}10^{-4}$ s^{-1} to $2.4\text{x}10^{-3}$ s^{-1}) is observed between the upper and lower limits of the strain rate for $L_{a0}/L_0 = 20$.

Conclusion

The mechanical response of 100 nm-thick freestanding copper films has been probed by means of on-chip MEMS-based internal stress actuated testing structures. Two actuator designs have been used: a classic rectangular design leading to a sequential, uncontrolled and very high strain rate, and a new tapered design allowing the control and estimation of the strain rate during the release step. The extracted stress-strain curves are superposed and do not reveal any strain rate sensitivity at the time of the measurement. They exhibit a Young's modulus of ~110 GPa and a yield stress of ~200

MPa. The two modelling strategies developed for the estimation of the upper and lower limits of the strain rate during the release have shown an increase from $1.5x10^{-5}$ s^{-1} to 1.3 - $1.9x10^{-4}$ s^{-1} between the least and the most deformed structures having a tapered actuator examined in this work.

Acknowledgments

Dr. Renaud Vayrette acknowledges the Fonds National de la Recherche Scientifique (FRS - FNRS) through the support of the project MECANO. The present work has been also carried out in the framework of the contract IAP 7/21 supported by the Interuniversity Attraction Poles Program from the Belgium State through the Belgium Policy Agency.

References

[1] M. Kasbari, C. Rivero, S. Blayac, F. Cacho, O. Bostrom, R. Fortunier, Direct Local Strain Measurements in Damascene Interconnects, Mater. Res. Soc. Symp. Proc. 990 (2007) 241-246.

[2] A. Boé, A. Safi, M. Coulombier, T. Pardoen, J.-P. Raskin, Internal stress relaxation based method for elastic stiffness characterization of very thin films, Thin Solid Films 518 (2009) 260-264.

[4] M.S. Baker, M.P. de Boer, N.F. Smith, L.K. Warne, M.B. Sinclair, Integrated Measurement-Modeling Approaches for Evaluating Residual Stress Using Micromachined Fixed–Fixed Beams, J. Microelectromech. Syst. 11 (2002) 743-753.

[5] J. Florando, W. Nix, A microbeam bending method for studying stress-strain relations for metal thin films on silicon substrates., J. Mech. Phys. Solids. 53 (2005) 619-638.

[6] B.D. Jensen, M.P. de Boer, N.D. Masters, F. Bitsie, D. A. LaVan, Interferometry of Actuated Microcantilevers to Determine Material Properties and Test Structure Nonidealities in MEMS, J. Microelectromech. Syst. 10 (2001) 336-346.

[7] M.A. Haque, M.T.A. Saif, Application of mems force sensors for in situ mechanical characterization of nano-scale thin films in SEM and TEM, Sens. Act. A 97-98 (2002) 239-245.

[8] M.A. Haque, M.T.A. Saif, Microscale materials testing using MEMS actuators, J. Microelectromech. Syst. 10 (2001) 146-152.

[9] H. Espinosa, Y. Zhu, N. Moldovan, Design and operation of a mems-based material testing system for nanomechanical characterization, J. Microelectromech. Syst. 16 (2007) 1219-1231.

[10] D. Fabrègue, N. André, M. Coulombier, J.-P. Raskin and T. Pardoen, Multipurpose nanomechanical testing machines revealing the size-dependent strength and high ductility of pure aluminium submicron films, Micro & Nano Lett. 2 (2007) 13-16.

[11] S. Gravier, M. Coulombier, A. Safi, N. André, A. Boé, J.-P. Raskin, T. Pardoen, New On-Chip Nanomechanical Testing Laboratory - Applications to Aluminum and Polysilicon Thin Films, J. Microelectromech. Syst. 18 (2009) 555-569.

[12] U. Bhaskar, V. Passi, S. Houri, E. Escobedo-Cousin, S.H. Olsen, J.-P. Raskin, T. Pardoen, On-chip tensile testing of nanoscale silicon free-standing beams, J. Mater. Res. 27 (2012) 571-579.

[13] M.-S. Colla, B. Wang, H. Idrissi, D. Schryvers, J.-P. Raskin, T. Pardoen, High strength-ductility of thin nanocrystalline palladium films with nanoscale twins: On-chip testing and aggregate model, Acta Mater. 60 (2012) 1795-1806.

[14] M. Coulombier, G. Guisbiers, M.-S. Colla, R. Vayrette, J.-P. Raskin, T. Pardoen, On-chip stress relaxation testing method for freestanding thin film materials, Rev. Sc. Inst. 83 (2012) 105004-105004-9.